Published in final edited form as:
Circ Res. 2010 July 9; 107(1): 126–137. doi:10.1161/CIRCRESAHA.110.219949.

Mechanistic links between Na+ channel (SCN5A) mutations and impaired cardiac pacemaking in sick sinus syndrome

Timothy D. Butters[*,1], **Oleg V. Aslanidi**[*,1], **Shin Inada**[2], **Mark R. Boyett**[2], **Jules C. Hancox**[3], **Ming Lei**[2], and **Henggui Zhang**[1]

[1]Biological Physics Group, School of Physics and Astronomy, University of Manchester, Manchester M13 9PL, United Kingdom

[2]Cardiovascular Research Group, Faculty of Medical and Human Sciences, University of Manchester, Manchester M13 9NT, United Kingdom

[3]Department of Physiology and Pharmacology, Cardiovascular Research Laboratories, Bristol Heart Institute, School of Medical Sciences, University of Bristol, Bristol BS8 1TD, United Kingdom

Abstract

RATIONALE—Familial sick sinus syndrome (SSS) has been linked to loss-of-function mutations of the SCN5A gene, which result in decreased inward Na^+ current, I_{Na}. However, the functional role of I_{Na} in cardiac pacemaking is controversial, and mechanistic links between the mutations and sinus node dysfunction (SND) in SSS are unclear.

OBJECTIVE—To determine mechanisms by which the SCN5A mutations impair cardiac pacemaking.

METHODS—Action potential (AP) models for rabbit sinoatrial node (SAN) cells were modified to incorporate experimentally reported I_{Na} changes induced by two groups of SCN5A gene mutations (affecting the activation and inactivation of I_{Na}, respectively). The cell models were incorporated into an anatomically detailed 2D model of the intact SAN-atrium. Effects of the mutations and vagal nerve activity on cardiac pacemaking at the single cell and tissue levels were studied. Multi-electrode extracellular potential recordings of activation pattern from intact SAN-atrium preparations were performed to test predictions of the models.

RESULTS—At the single cell level, the mutations slowed down pacemaking rates in peripheral, but not in central SAN cells that control the heart rhythm. However, in tissue simulations, the mutations not only slowed down pacemaking, but also compromised AP conduction across the SAN-atrium, leading to a possible SAN exit block or sinus arrest, the major features of SSS. Simulated vagal nerve activity amplified the bradycardiac effects of the mutations. Two groups of SCN5A mutations showed subtle differences in impairing the ability of the SAN to drive the surrounding atrium – primarily, due to their differential effects on atrial excitability and conduction safety. Experimental data with tetrodotoxin and carbachol confirmed the simulation outcomes.

Correspondence to: Professor Henggui Zhang Tel: 44 (0)161 306 3966; henggui.zhang@manchester.ac.uk**or** Dr. Ming Lei Tel: 44(0)161 275 1194; ming.lei@manchester.ac.uk.
*Joint first authors

Disclosures None of the authors of the present manuscript has any disclosures to declare.

CONCLUSIONS—Our study substantiates the causative link between SCN5A gene mutations and SSS, and illustrates mechanisms by which the mutations impair the driving ability of the SAN.

Keywords

Sick sinus syndrome; SCN5A mutation; ion channels; computer modelling

1. INTRODUCTION

Sick sinus syndrome (SSS) denotes a collection of cardiac arrhythmias associated with dysfunction of the sinoatrial node (SAN) that commonly lead to disorders in cardiac rhythm and conduction.[1] Such arrhythmias include intermittent sinus bradycardia, sinus arrest, sinus pause, slow SAN-atrium conduction, sinus exit block or alternating bradycardia and atrial tachycardia.[1-4] The symptoms of SSS vary, with patients presenting with syncope, presyncope, palpitations or dizziness.[1,5] Many SSS patients have to be fitted with an electronic pacemaker.

Mechanisms underlying the pathogenesis for sinus node dysfunction (SND) in SSS patients are unclear. SSS can occur in elderly and paediatric patients. It can also occur in healthy people without any evident structural heart disease,[2,4] but with genetic defects. Recent studies have identified several gene mutations in congenital SSS patients.[2,4,6,7] Among them are the SCN5A gene mutations that alter the pore-forming structure of the α-subunit of the cardiac Na^+ channel. In congenital SSS families, Benson *et al.*[2] identified several SCN5A mutants that include threonine in place of isoleucine at position 220 (T220I), leucine in place of proline at position 1298 (P1298L) and in-frame deletion (delF1617) mutations. Functional analysis of the expression of the wild-type (WT) and mutant Na^+ channels in cultured mammalian cell line (tsA201) revealed that these mutations resulted in reduced I_{Na} current density, together with impaired fast inactivation (*i.e.*, a shift in the voltage-dependent steady-state inactivation curve to a more hyperpolarizing potential) in comparison to the WT channel.[2] Smits *et al.*[6] identified another SCN5A mutation associated with SSS – replacement of glutamine by lysine at position 161 (E161K) mutation. Functional analysis of the E161K mutation also revealed reduced I_{Na} current density. However, in contrast to T220I, P1298L and delF1617 mutations, the E161K mutation caused a shift in the steady-state activation curve to a more depolarized potential. Although all these SCN5A mutations share in common a reduction in I_{Na}, they are intrinsically different in their kinetic effects and can be classified into two distinctive groups, one altering I_{Na} inactivation (G1: T220I, P1298L and delF1617) and the other altering I_{Na} activation properties (G2: E161K). At the macroscopic level, a negative shift in voltage-dependent inactivation or a positive shift of voltage-dependent activation may have similar consequences in terms of reducing the I_{Na} 'window' current. However, they may modulate differently cardiac excitability, and thus, differentially affect the ability of the SAN to pace and drive the surrounding atrial muscle.

The loss-of-function of I_{Na} due to SCN5A mutations is also associated with other cardiac diseases that include Brugada syndrome and progressive cardiac conduction system disease.[6,8,9] However, the mechanistic link between loss-of-function of I_{Na} arising from these mutations and impaired SAN function has not been elucidated. Primarily, whether and how these mutations compromise the ability of the SAN to drive the surrounding atrial muscle has not been investigated, as the existing experimental studies are limited to molecular and ionic levels.[2,6,10,11] Furthermore, the role of Na^+ channels in cardiac pacemaking is still controversial,[7,12-14] as the channels are expressed in peripheral SAN cells, but either completely absent or dramatically less-expressed in central SAN cells which mainly control the cardiac rhythm.[7]

Europe PMC Funders Author Manuscripts

Computational models provide a powerful way to study the functional effects of reduced I_{Na} in initiation and conduction of the pacemaking action potential (AP), an emergent dynamical behaviour of coordinated ion channels and inter-cellular electrical coupling.[6,14-17] Smits *at al.*[6] have shown that the E161K mutation slows down the pacemaking rate in a peripheral SAN cell model,[15] and AP conduction in a one-dimensional atrial strand model. Both effects were enhanced by acetylcholine (ACh), the neurotransmitter released by the vagal nerves. However, the mechanisms by which the loss-of-function of I_{Na} slows down the heart rate in the intact SAN-atrium (in which the heart rate is mainly controlled by central SAN cells with little or no I_{Na}, rather than peripheral SAN cells) and impairs AP conduction from the SAN to the atrial tissue (*i.e.*, the ability of the SAN to drive the surrounding atrium) have not been fully elucidated. It is also unclear whether or not the two distinctive mutation groups (G1 and G2) exhibit similarity or difference in their functional impacts. The aim of this study was to address these issues.

2. METHODS

The consequences of the impaired I_{Na} channel function due to several SCN5A mutations (T220I, P1298L, delF1617 and E161K) in generating SND were investigated by using (i) previously developed electrophysiologically detailed mathematical models of the central and peripheral SAN[15] cells, (ii) two-dimensional (2D) anatomical models of the intact SAN-atrium tissue, incorporating accurate single cell models of the SAN[15] and the right atrium (RA),[18] and histologically reconstructed tissue geometry,[19] and (iii) multi-electrode extracellular potential recordings of the activation pattern from isolated intact rabbit SAN-atrium tissue to verify model predictions.

A full list of the model equations and parameters used for the central and peripheral SAN cells and RA cells under control conditions, SCN5A mutation conditions and ACh conditions, as well as 2D tissue model of the intact SAN-atrium, is provided in the Online data supplement. Electronic copies of the respective codes are also available upon request.

2D slice model

The 2D model of intact SAN-atrium tissue used in this study was based on histologically reconstructed[19] geometry of a single slice of the rabbit RA, which was cut through the atrial muscle of the crista terminalis (CT) and the intercaval region with central and peripheral SAN areas (Fig. 1A). The geometry presents a high spatial resolution (40 μm, which corresponds to 2 to 4 diameters of a cardiac myocyte) regular Cartesian grid of 210×45 nodes. For each node, a flag variable was used to identify whether it belongs to the SAN or RA cell type based on immunohistochemistry mapping data.[19] The SAN was modelled by the Zhang *et al.* equations[15] for central and peripheral cells, and the RA was modelled by the Aslanidi *et al.* equations[18] for atrial cells, with each model producing different AP morphology (Fig. 1A).

The model also incorporated an experimentally observed[19,20] non-conductive region ("block zone") next to the SAN towards the atrial septum, where cells have low excitability. The AP conduction in the 2D tissue model due to intercellular electrical coupling via gap junctions was modelled through the diffusion coefficient, D. In the model, we considered the regional differences in the cellular electrophysiological properties and gap junctional coupling between the SAN centre, periphery and atrial tissue as observed experimentally.[19] A spatial gradient of D (Fig. 1F) was introduced as in our previous study.[17] The gradient distributions of current densities from the central to the peripheral SAN were modelled by correlating them to cell membrane capacitance, C_m, which was assumed to be small in the centre and large in the periphery.[12,15,17] Spatial variations in all ion channel conductances were defined

as a function of C_m as found experimentally.[15] Full equations are presented in the Online data supplement.

The single cell models for SAN central and peripheral cells and RA cells have been validated in our previous studies.[15],[18] The developed 2D anatomical model of the intact SAN-atrium was validated by its ability to reproduce the correct sequence of AP initiation and conduction through the rabbit SAN-atrium, as observed experimentally[20],[21]. In the 2D model, the pacemaking AP was first initiated in the centre of the SAN (Figs. 1B and 1C), and it then propagated preferentially towards the CT; AP conduction towards the atrial septum was relatively slow. The space-time plot of the AP profiles recorded from cells along a line across the SAN-atrium (Fig. 1D) showed continuous AP initiation and conduction. The computed activation time of the CT (1.5 mm distance from the centre of the SAN) matched quantitatively to experimental data (Fig. 1C), which validates the intercellular electrical coupling used in the model. Simulation results with the 2D model were also validated against respective experimental data from isolated rabbit SAN-atrium (see below).

SCN5A mutation model

In order to model SCN5A mutations from G1 (T220I, P1298L and delF1617), parameters of the fast Na^+ current, I_{Na}, were changed to reproduce experimental data (Fig. 2). Note that prior experimental data[2] were recorded from tsA201 cells transfected with a recombinant human Na^+ channel cDNA (hH1), whereas our models are for the native current in rabbit SAN cells. Thus, in simulations we shifted the steady-state inactivation curve by the same amount as observed experimentally (Figs. 2C and 2D) and implemented the same percentage changes of the fast- and slow-inactivation time constants as observed experimentally (Fig. 2A). We scaled the maximal I_{Na} channel conductance by a factor S_{CD} (see Online Table I) to reproduce the normalised I-V relationship (Fig. 2E) and the reduction in I_{Na} as observed experimentally (Fig. 2F). The heterozygous E161K mutation was modelled by the same method as used by Smits *et al.*[6] I_{Na} was divided into two components – one for the WT I_{Na} and another for the E161K mutant I_{Na} The WT component had a maximum conductance of 50% of control, whereas the mutant component had a maximum conductance of 20% of control. The steady-state activation curve of the mutant component was also shifted by 11.9 mV (Fig. 2B). Full equations are presented in the Online data supplement.

Isolated tissue experiments

5 male adult rabbit (2-3 months old) were used for experimental study. The sino-atrial preparations were set up as described previously from animals killed by anesthetic overdose with venous injection of sodium phenobarbital (in accord with UK Home Office Legislation).[22] After excision of the SAN and surrounding atrial muscle, the preparation was placed endocardial surface upwards in a tissue bath and superfused with modified Tyrode's solution (in mmol/L: NaCl 120, $NaHCO_3$ 25.2, NaH_2PO_4 1.2, $MgCl_2$ 1.3, glucose 5, KCl 4.0, $CaCl_2$ 1.8, gassed with 95% O_2/5% CO_2) at 37 °C and at a flow rate of ~5 ml/min. Electrical signals were obtained from the surface of this preparation by apposition of a custom-made extracellular multi-electrode array that allowed electrograms to be monitored at multiple sites in the tissue as excitation passed under the array. The electrode array held 30 separate silver electrodes in a 5×6 configuration (a detailed description of the electrodes is presented in the Online data supplement). The 30 recording electrodes were connected through shielded wires to a 32-channel amplifier (SCXI-1102C, National Instruments Corporation UK Ltd, Newbury, UK). The sampling frequency for each channel was set at 1 kHz. The signals were continuously sampled and stored on disk and displayed on screen using a custom-developed program, written in Labview 7.0 (National Instruments Corporation UK Ltd, Newbury, Berks RG14 2PS, UK). Experiments were performed under the conditions of control, application of tetrodotoxin (TTX) (0.5 μmol/L; IC_{50} ~ 0.1 μmol/L

[23]) or a non-degrading ACh equivalent – carbachol (CCh) (200 nmol/L; IC_{50} ~ 100 nmol/L [24]), and a combination of TTX (0.5 μmol/L) and CCh (200 nmol/L). Propagation maps were then derived during off-line analysis. The signals were displayed on screen in sets of 8 to 16 electrograms. The activation time was denoted as the point of maximal negative slope and marked with a cursor. After marking all significant waveforms in all leads, the activation times were then displayed in a grid representing the layout of the original recording array. All activation times, in milliseconds, were related to the timing of the first detected waveform.

3. RESULTS

Mutation effects on single cells

At the single cell level, the central and peripheral SAN cell models were used to investigate the functional effects of the SCN5A mutations (G1: T220I, P1298L and delF1617; G2: E161K) on AP generation under control and ACh conditions. Figs. 3A-D show effects of the P1298L mutation, and Fig. 3E summarises quantitative effects of all mutations. Figs. 3A-D show simulated AP with the WT and P1298L mutant channels, along with major underlying ionic currents in the central (left panels) and peripheral (right panels) cells. These simulations illustrate that the P1298L mutation did not affect the central cell (Fig. 3Ai), but it dramatically slowed down pacemaking in the peripheral cell (Fig. 3Aii) – the pacemaking cycle length (PCL) increased from 170 to 204 ms, an increase of 19.7%. This is similar to experimental observations by Honjo *et al.*,[12] who reported that blocking I_{Na} with TTX did not affect central cells, but slowed pacemaking of peripheral cells in the rabbit SAN. In the model, the resultant slowing down of the pacemaking was primarily due to the mutation-induced decrease in I_{Na} (Fig. 3Bii), as other major underlying currents (such as $I_{Ca,L}$ and $I_{K,r}$) were not greatly affected (Fig. 3Cii, 3Dii). Functional effects of other mutations were similar: there was a slowing of pacemaking in peripheral cells and an increase of the PCL by 7.1%, 10.8%, 19.1% and 7.1% for the T220I, delF1617 and E161K mutations, respectively (Fig. 3Eii).

ACh effects on single cells

Application of ACh slowed down pacemaking by increasing the PCL in both central and peripheral SAN cells, with a larger effect on the central cells.[16] Simulating effects of 5×10^{-8} mol/L ACh resulted in the PCL increasing from 338 ms to 429 ms (27.1% increase) for the central SAN cell, and from 171 ms to 194 ms (13.7% increase) for the peripheral SAN cell. The negative chronotropic effect of ACh was due to an integral action of $I_{K,ACh}$ (Fig. 4B) and changes in $I_{Ca,L}$ (Fig. 4C) and I_f (Fig. 4D). When the P1298L mutation was considered, the negative chronotropic effect of ACh was amplified for the peripheral cell model, but it remained the same for the central cell model (Fig. 4A). The augmented negative chronotropic effects of ACh with the mutant channel can be attributed to the reduced inward depolarizing I_{Na} during the diastolic depolarization period, which counter-balances the ACh-activated outward repolarizing current, $I_{K,ACh}$, leading to a greater slowing of the diastolic depolarization. Such behaviour was also observed for other SCN5A mutations. With the same 5×10^{-8} mol/L ACh concentration, the PCL in the peripheral cell model increased by 26.0%, 50.4%, 45.3% and 23.4% with the T220I, P1298L, delF1617 and E161K mutations respectively, which is markedly greater than with the WT channel (13.7%).

The dose-dependent effects of ACh on pacemaking APs with the WT and mutant channels were also simulated. Fig. 5 presents results obtained from the peripheral cell model for different ACh concentrations with the WT (Fig. 5A, C and E) and the P1298L mutant (Fig. 5B, D and F) channels. It shows that increase in ACh concentration led to a greater increase in PCL, and the negative chronotropic effect was amplified by the P1298L mutation at all

ACh concentrations. At an ACh concentration of 15×10^{-8} mol/L (Fig. 5E), the cell with the WT channel still exhibited pacemaking (though with prolonged PCL), but the cell with the mutant channel became quiescent. Fig. 5G summarises the simulated dose-dependent effect of ACh on pacemaking APs with the WT and various mutant channels. It shows that all the mutations shifted the dose-dependence of the PCL leftward, indicating a more suppressive effect of ACh on SAN cells incorporating 'mutant' I_{Na}. The dose-dependent effects of ACh on pacemaking at the 2D tissue level are illustrated in Fig. 5H.

2D tissue effects

We investigated further the functional consequences of the mutations on AP conduction across the intact SAN-atrium under control and ACh conditions. Results are shown in Fig. 6, which presents the spatial (running horizontally) and temporal (running vertically) profiles of APs recorded from representative cells across the SAN-atrium model in Fig. 1A. Fig. 6A presents the normal conduction in the normal tissue (with the WT channel and no ACh). Simulation of ACh addition (1.5×10^{-8} mol/L) slowed down the pacemaking rate (*i.e.*, led to an increase in the PCL) (Fig. 6B). Fig. 6C shows the AP profile with the P1298L mutation, a representative of the G1 group. Without ACh, the mutation slowed down the pacemaking rate, but did not impair the ability of the SAN to drive the atrium. However, with ACh the SAN pacemaker activity was abolished (Fig. 6D) and, thus, the SAN lost the power to drive the atrium. Fig. 6E and F show the effects of the G2 E161K mutation. Without ACh, the mutation slowed down pacemaking, and also produced a conduction block in the direction towards the atrial septum; however, the AP conduction in the direction towards the CT was sustained. With an ACh concentration of 1.5×10^{-8} mol/L, the SAN was able to generate spontaneous activity, but failed to drive the surrounding atrium – conduction exit block occurred in both directions.

Detailed simulations were also performed to investigate the effects of the mutations and ACh on the characteristics of AP initiation and conduction in the intact SAN-atrium tissue model. Fig. 7A presents the measured activation timing sequence across the tissue with the WT and E161K mutant channels, with and without ACh. In the model, simulated application of ACh or the E161K mutation alone increased the time required for the AP to propagate from the centre of the SAN to the RA, *i.e.*, the SAN conduction time (Fig. 7A). The E161K mutation alone resulted in AP conduction failure in the direction towards the atrial septum. Furthermore, when ACh addition was simulated, there was a dramatic delay in AP initiation and also conduction block both towards the CT and the septum. However, the P1298L mutation markedly delayed AP initiation (Fig. 7B), but did not increase the SAN conduction time; addition of ACh completely abolished the AP.

The measured AP conduction velocity in SAN-atrium tissue simulations also reflected the above observations. In the normal tissue with the WT channel, addition of ACh reduced the conduction velocity by ~12% in the SAN (on average) and by ~7% in the RA (Fig. 7C). In tissue with the E161K mutant channel, the conduction velocity was decreased by ~46% in the SAN (on average) and by ~45% in the RA (Fig. 7C). Subsequent addition of ACh to the tissue with the E161K mutant channel further reduced the AP conduction velocity in the SAN, and resulted in a complete conduction block in the atrium. In tissue with the P1298L mutant channel, the AP conduction velocity was decreased by ~8% in the SAN (on average), and by ~8% in the RA (Fig. 7D); subsequent addition of ACh abolished pacemaking (Fig. 7D).

Changes in the measured conduction velocity across the SAN-atrium were attributed to the changed maximum upstroke velocity (dV/dt_{max}), as shown in Fig. 7E, F. In the normal tissue with the WT channel, simulated addition of ACh reduced dV/dt_{max} in both the RA and the SAN, with a greater effect on the RA. In tissue with the E161K mutant channel,

there was a decrease in dV/dt_{max} throughout the tissue (up to ~27%), not only in the RA and periphery of SAN, but also in the centre of the SAN; subsequent addition of ACh further reduced dV/dt_{max} in the SAN, with more dramatic effects in the SAN periphery, primarily at the border between the SAN and the atrium. This resulted in the SAN failing to drive the atrium, leading to SAN exit block. The P1298L mutation reduced dV/dt_{max} markedly in the SAN region, but only slightly in the RA region. Addition of ACh to tissue with the P1298L mutant channel (Fig 7F) abolished pacemaking and dV/dt_{max} was zero throughout the SAN (data not shown).

Effects on excitability and conduction safety

We have measured the excitation threshold, a reciprocal measure of cardiac excitability, for atrial cells in WT and mutant cases. Both the G1 and G2 mutations reduced atrial excitability, but to different extents. For the P1298L and E161K mutations, the measured excitation threshold increased from 1.7 to 2.1 and 2.8 nA, respectively, for a stimulus pulse duration of 1 ms. With simulated ACh addition, the respective changes were from 2.8 with the WT channel to 3.0 and 4.1 nA with the P1298L and E161K mutant channels. Thus, both mutations and ACh increased the excitation threshold for atrial cells. The larger increase of the excitation threshold associated with the G2 group (E161K) was correlated with higher vulnerability of the tissue to AP conduction block at the junction of the SAN-atrium (see Online Fig. I).

Large differences in the magnitude of the threshold increase can be explained by the different nature of the mutations: although both the P1298L and E161K mutations result in about the same reductions in the current density of I_{Na} (Fig. 2E, F), but the underlying kinetic changes are different. P1298L represents a family of mutations that cause hyperpolarizing shifts in the steady-state inactivation curve (Fig. 2C), whereas E161K causes a depolarizing shift in the steady-state activation curve (Fig. 2B). Both shifts decrease the window current, but only E161K substantially increased the excitation threshold, which is sensitive primarily to the activation kinetics of I_{Na}. Results of a systematic analysis of effects of activation and inactivation shifts on excitability are presented in the Online supplement (see Online Fig. I).

Na^+ channel defects that result in decreased tissue excitability have been associated with reduced AP conduction safety manifested as decreases in the safety factor (SF).[25] Our simulations of SF changes (see the Online data supplement for details) due to effects of the SCN5A mutations and ACh suggested that the G2 (E161K) mutation results in a greater decrease of SF arising from greater decreased tissue excitability as compared to G1 mutations (Online Fig. II). Importantly, the AP conduction block due to the effects of the E161K mutation and high ACh concentration can be localized close to the exit site from the CT towards the RA (see Online Fig. II), where low SF emerges from a combination of both electrophysiological (high excitation threshold, low dV/dt_{max}) and geometrical (high source-to-load mismatch due to narrowing of the tissue) factors.

Experimental validation

Multi-electrode extracellular recordings of AP initiation and conduction pattern in isolated rabbit SAN-atrium tissue were performed experimentally to verify simulation results with the 2D tissue slice model (Fig. 6). Due to lack of phenotypically accurate rabbit models, defective I_{Na} by the SCN5A variants was mimicked by reducing I_{Na} through the application of TTX. Fig. 8 shows the electrical activation maps of the intact SAN-atrium tissue reconstructed from extracellular potentials recorded from the endocardial surface of the SAN-atrium preparation (see Methods). In control, the excitation was generated in the SAN centre and propagated towards the RA with an average AP conduction velocity in the

direction transverse to the CT of 0.12 m/s. In terms of the AP conduction velocity, application of 0.5 μmol/L TTX alone slowed it down to 0.08 m/s; whilst application of 200 nmol/L CCh alone did not have any significant effect on the velocity. However, combined application of 0.5 μmol/L TTX and 200 nmol/L CCh resulted in a much more substantial slowing of the AP conduction than TTX alone, down to 0.05 m/s. In terms of pacemaking rhythm, application of CCh or TTX alone resulted in an increase in the PCL from 340 to 430 and 380 ms, respectively. However, combined application of TTX and CCh increased the PCL to 490 ms. The experimentally measured changes in both the AP conduction velocity and PCL are in good agreement with the simulation results (Fig. 8), thereby supporting the predicted roles of SCN5A variants and the accentuating effects of ACh on impairing the cardiac pacemaker.

4. DISCUSSION

In this study, we have developed a family of SAN cell models with WT and mutant SCN5A channels, and incorporated them into an electrophysiologically and anatomically detailed 2D computer model of the rabbit SAN and surrounding atrium. Using the model, we investigated the functional effects of two groups of SCN5A mutations (G1 and G2) in impairing the ability of the SAN to pace and drive the surrounding atrial muscle. Functional differences between the two mutation groups were also studied. Our major findings are as follows: (1) At the intact SAN-atrium tissue level, I_{Na} reduction due to the SCN5A mutations slowed down pacemaking and compromised the AP conduction across the SAN-atrium, leading to a possible sinus arrest or SAN exit block, which are major features of SSS. Our simulation results provide evidence substantiating the causative link between familial SSS and the identified gene mutations. (2) The functional impacts of reduced I_{Na} at the isolated single cell level are different to those seen in the intact SAN-atrium tissue level. Such a discrepancy is attributable to electrotonic interaction between the SAN and atrium. Thus, single cell simulations cannot be relied on solely, and multicellular tissue models must be used to evaluate the functional role of I_{Na} in cardiac pacemaking. (3) The bradycardiac effects of the SCN5A gene mutations are likely to be amplified by vagal nerve activity: simulated addition of ACh to the tissue with a mutant channel not only slowed pacemaking and AP conduction, but also compromised the ability of the SAN to pace and drive the atrium, leading to a higher probability of sinus arrest and SAN exit block than with the mutations or ACh alone. This finding agrees with that of Smits *et al.*[6] and may provide further insight into the mechanism underlying high risk of cardiac arrest in SSS patient at night, when vagal tone is greater.[26,27] (4) The two groups of SCN5A mutations (G1 and G2) show common features in impairing the pacemaking ability of the SAN and the AP conduction across the SAN-atrium, but have subtle differences in affecting the ability of the SAN to drive the surrounding atrium. This is due to their different impacts on atrial excitability. (5) SAN exit block occurred due to the combined effect of SCN5A mutations and ACh, which produces a decreased SF in the local region close to the exit site from the CT towards the RA, where the source-to-load mismatch is the largest due to both electrophysiological and geometrical factors. (6) Our simulation results are supported by experimental data, collectively indicating an important role for cholinergic activity in accentuating the deleterious effects of defective Na^+ channels on cardiac pacemaking. Taken together, these findings enhance current understanding of the mechanistic links between the studied SCN5A gene mutations and the resultant anomalies of cardiac pacemaker.

SCN5A mutations and pacemaker abnormalities

Our study has shown that, at the isolated single cell level, all the considered SCN5A mutations slowed pacemaking of peripheral SAN cells, but not central SAN cells that normally initiate and control the heart rhythm. However, at the intact SAN-atrium tissue

level, the SCN5A mutations slowed down the heart rate by slowing down pacemaking in the central cells, which have no I_{Na}. This can be attributed to the electrotonic interaction between the SAN and the atrium. Due to a hyperpolarized resting potential (more negative than the maximal diastolic potential of the SAN) and lack of pacemaking activity, the atrium acts as an electrical load suppressing the pacemaker activity of the SAN. Such a suppressive action can be mapped to the centre of the SAN through cell-to-cell electrical coupling, although its effects here are weaker than in the periphery. With the mutations, the suppressive action becomes greater as less I_{Na} is available to counterbalance the suppressive effect of adjacent atrial tissue.[28]

Our simulations also showed that the mutations slowed AP conduction across the SAN-atrium. As shown by the activation time profiles (Fig. 6), the AP conduction through the SAN is slow with all mutations, as often reported in SSS patients or patients with other cardiac conditions linked to mutations in the SCN5A gene.[6],[10] This is considered a sign of potential conduction failure risks, *e.g.* sinus exit block.[1] Conduction block was observed in our simulations with the E161K mutation (Fig. 6E), in agreement with clinical observations.[6] The block can be accounted for by a combination of decreased atrial excitability (Online Fig. I) and conduction safety (Online Fig. II), which are most prominent with the E161K mutation.

Acetylcholine effects

Addition of ACh slowed pacemaking in both the single cell and 2D simulations, as did CCh in experiments; the negative chronotropic effect of ACh was greater with the SCN5A mutant channels than with the WT channel. The augmented bradycardiac effect of ACh can be attributed to the associated reduction of I_f (Fig. 4). Without ACh, reduced I_{Na} leads to a more hyperpolarized membrane potential in SAN cells, which activates more I_f. This increase in I_f counter-balances the reduced I_{Na} in the diastolic phase. However, as I_f is reduced by ACh, its counter-balancing effect on I_{Na} is also reduced, which results in the observed augmented negative chronotropic effect.

Note that cholinergic receptor stimulation by ACh also reduces $I_{Ca,L}$, the effect ascribed to a PKA-dependent reduction in L-type Ca^{2+} channel phosphorylation, which can occur either during β-adrenoreceptor stimulation,[29] or in its absence.[30] However, it remains controversial whether ACh inhibitory effects on $I_{Ca,L}$ do occur in the absence of concurrent β-adrenoreceptor stimulation. Recent findings[24] have shown that in the absence of β-adrenergic stimulation CCh reduced the $I_{Ca,L}$ amplitude by 20% - but only at a 10-fold higher [CCh] than that required to stop pacemaking; effects of lower [CCh], corresponding to physiologically feasible ACh levels, were much smaller. In our model, the description of the dose-dependence of $I_{Ca,L}$ on [ACh] has been based on similar data.[16],[30] Consequently, modulation of $I_{Ca,L}$ by "physiological" [ACh] considered in our study is weak; removing this modulation from the model has not changed qualitative results of our simulations (quantitative changes to the pacemaking rate and AP conduction velocity were <10%). Obviously, in the evenings when effects of the sympathetic nervous system on the heart rate (primarily, the pacemaking rate and AP conduction velocity) via β-adrenoreceptor are reduced, modulation of $I_{Ca,L}$ by ACh will be weaker than during daytime. However, effects of such a reduction of $I_{Ca,L}$ modulation on the heart will be much smaller that those due to ACh activation of $I_{K,ACh}$.

Our simulations demonstrate that ACh not only slows down pacemaking as observed in single cell studies,[2],[6] but also impairs the ability of the SAN to drive the surrounding atrial muscle – as revealed by our 2D simulations (Fig. 6), and verified in isolated SAN-atrium tissue experiments (Fig. 8). Thus, increased vagal nerve activity (leading to greater ACh release onto the SAN) can be anticipated to augment the bradycardic effects of the SCN5A

mutations. This result is also validated experimentally (Fig. 8), and is consistent with clinical observations that significantly lower heart rates occur at night, when vagal tone is high.

Previous modelling studies

Note that our study of the conditions of compromised AP conduction in the SAN-atrium tissue and their mechanistic links with the SSS is related to, but distinct from the previous results by Kurata *et al.*[31] The latter study focused on bifurcation structures of several single cell models: (i) SAN cells under high [ACh] effects; (ii) SAN cells electrotonically coupled to atrial cells via conductance G_C; (iii) models (i) and (ii) with blocked I_{Na}. When I_{Na} was not blocked, the cells exhibited robust pacemaking over broad ranges of [ACh] and G_C values; pacemaking cycle lengths increased as [ACh] and G_C increased.[31] However, I_{Na} block dramatically shrunk the [ACh] and G_C parametric regions corresponding to spontaneous pacemaking, suggesting that I_{Na} is important for maintaining the relatively high structural stability of the system consisting of coupled SAN and atrial cells. Whilst distinct, these observations are consistent with our results, primarily on the effects of I_{Na} impairment, ACh and electrotonic load from the atrium on the pacemaking rate (Fig. 5). Besides, simulations of our 2D tissue model show that the loss of structural stability in the coupled-cell model[31] corresponds to failure of the SAN to pace and drive atrial tissue (Fig. 6), the effect being due to a combination of SCN5A Na^+ channel mutations and high [ACh]. The AP conduction from the SAN into the RA is compromised as the combined effects of I_{Na} impairment and activation of $I_{K,ACh}$ substantially increase the tissue excitation threshold (Online Fig. I). These results are verified experimentally (see Fig. 8): whilst CCh alone did not have a significant effect on the AP conduction velocity, a combination of TTX (which suppresses I_{Na}) and high [CCh] resulted in much slower conduction in SAN-atrium preparations than TTX alone.

Limitations

Limitations of cardiac cell and tissue models are well documented.[15],[18] In our single cell model development, we modified the equations for I_{Na} based on available experimental data from cultured tsA201 cells.[2] As our models are for rabbit cells and tissue, relative shifts between the WT and mutant parameters (such as the current density, the inactivation time constants and the steady-state inactivation curve of I_{Na}) were calculated from the experimental data, and applied in the rabbit model. Here we made an explicit assumption that rabbit Na^+ channel characteristics would show changes in response to SNC5A mutations that would be proportionately similar to those for human Na^+ channels. The fact that our model utilises cross-species data is not unusual; this is a common practice in cardiac modelling in situations where complete data from a single species are often unavailable. Note also that data by Benson *et al.*[2] have been recorded from patients with heterozygous SCN5A mutations. Such mutations can be modelled by the same method as used by Smits *et al.*[6], with I_{Na} divided into two components – one for the WT and another for the mutant I_{Na} – and each component having a maximum conductance of 50% of control. We have observed that such models of the heterozygous SCN5A mutations from G1 group produce results (not shown) that are qualitatively similar to those reported above. Another notable feature of the present study is that, due to the lack of phenotypically accurate rabbit models, in our *in vitro* experiments defective Na^+ channel function with SCN5A variants was mimicked pharmacologically – by reducing I_{Na} through the application of TTX. Nevertheless, there was good concordance between experimental and simulation findings (see Fig. 8).

Our 2D anatomical tissue model is only a portion of the whole atria of the rabbit. 3D geometry[19] may ultimately be required to study patterns of the AP generation and

conduction in the SAN (e.g., exact locations of the sinus exit block sites, including the established block zone towards to atrial septum), which may depend on details of the tissue spatial structure, 3D heterogeneity and anisotropy. The dimensions of our tissue model have been reduced from full 3D to 2D, as we were primarily interested in interaction between the centre and periphery of the SAN during pacemaking and following AP conduction from the SAN across the CT into the RA. These phenomena can be studied within a slice, where main 3D geometrical features of the SAN-atrium tissue are projected onto a 2D plane transversal to the CT. That our approach of using a 2D slice is reasonable is borne out by experimental data verifying our simulation results (Fig. 8).

Mechanisms of SSS

Our simulations show that different mutations of the same gene (SCN5A) can lead to different modes of SAN dysfunction: abnormally slow pacemaking (with all mutations; enhanced by ACh), failure of the SAN to pacemake (G1: with T220I, P1298L and delF1617 mutations at high ACh concentrations) or sinus exit block (G2: with E161K mutation). All these behaviours are typical of SSS.[1,4] Although an exaggeration of the normal ageing process through factors such as degenerative fibrosis could also be an important cause, it is clear that ion channel mutations underlie the familial disease.[3] As well as SCN5A mutations, other ionic channel defects (such as mutations in the HCN4 gene encoding the hyperpolarization-activated cyclic nucleotide gated channel generating the pacemaking current, I_f [4]) can also cause SSS. In cases where such mutations lead to abnormalities in AP rate and conduction, computational techniques similar to those employed here may be used to provide mechanistic links between ion channel mutations and SSS.

Novelty and Significance

What is known

- Sick sinus syndrome (SSS) is a collection of cardiac arrhythmias associated with dysfunction of the cardiac primary pacemaker – the sinoatrial node (SAN).
- Recent studies have identified several gene mutations in congenital SSS patients. Among them are mutations of the SCN5A cardiac Na^+ channel.
- It is still unclear how SCN5A mutations compromise the ability of the SAN to pace and drive the surrounding atrial muscle in SSS patients.

What new information does this article contribute?

- At the single cell level, SCN5A mutations slow down pacemaking rates in peripheral, but not in central SAN cells that control the heart rhythm.
- In the SAN-atrial tissue, the mutations not only slow down pacemaking, but also slow down the conduction across the SAN-atrium, leading to a possible SAN conduction exit block or sinus arrest, the major features of SSS.
- Vagal nerve activity amplifies the bradycardiac effects of the SCN5A mutations; it also compromises the ability of the SAN to pace and drive the atrium, leading to a higher probability of sinus arrest or SAN exit block than with the mutations alone.

Summary

The role of SCN5A gene mutations in compromising the ability of the SAN to drive the surrounding atrial muscle in SSS patients has hitherto been unclear. We sought to address this issue using cell and tissue mathematical models. Our major findings are: (1) Reduction of Na^+ channel current due to the SCN5A mutations slows down both

pacemaking and conduction across the SAN-atrium, leading to a possible sinus arrest or SAN exit block, the major features of SSS. (2) The functional impacts of reduced Na^+ current at the isolated single cell level differ from those seen at the intact SAN-atrium tissue level, at which electrotonic interactions occur between the SAN and atrium. (3) The bradycardic effects of the SCN5A mutations are amplified by vagal activity, increasing the probability of sinus arrest and SAN exit block. (4) Simulation data were supported by experimental data from isolated rabbit SAN-atrium tissue. For the first time, these findings illustrate mechanisms by which the SCN5A gene mutations impair the driving ability of the SAN. Our results are consistent with clinical observations and may provide new insights into the mechanisms underlying high risk of cardiac arrest in SSS patients at night, when vagal tone is greater.

Supplementary Material

Refer to Web version on PubMed Central for supplementary material.

Acknowledgments

Sources of Funding This work was supported by a project grant (BBS/B/1678X) from the Biotechnology and Biological Sciences Research Council (UK), a Doctoral Training Account from the Engineering and Physical Sciences Research Council (UK) and the Wellcome Trust UK grant (WT/081809/Z/06/Z).

Non-standard Abbreviations and Acronyms

ACh	acetylcholine
AP	action potential
CCh	carbachol
CT	crista terminalis
IVC	inferior vena cava
G1	Group 1 mutations
G2	Group 2 mutations
PCL	pacemaking cycle length
RA	right atrium
SAN	sinoatrial node
SF	safety factor
SND	sinus node dysfunction
SSS	sick sinus syndrome
SVC	superior vena cava
TTX	tetrodotoxin
WT	wild type

REFERENCES

1. Adan V, Crown LA. Diagnosis and treatment of sick sinus syndrome. Am Fam Physician. 2003; 67:1725–1732. [PubMed: 12725451]

Europe PMC Funders Author Manuscripts

2. Benson DW, Wang DW, Dyment M, Knilans TK, Fish FA, Strieper MJ, et al. Congenital sick sinus syndrome caused by recessive mutations in the cardiac sodium channel gene (SCN5A). J Clin Invest. 2003; 112:1019–1028. [PubMed: 14523039]
3. Dobrzynski H, Boyett MR, Anderson RH. New insights into pacemaker activity: Promoting understanding of sick sinus syndrome. Circulation. 2007; 115:1921–1932. [PubMed: 17420362]
4. Schulze-Bahr E, Neu A, Friederich P, Kaupp UB, Breithardt G, Pongs O, et al. Pacemaker channel dysfunction in a patient with sinus node disease. J Clin Invest. 2003; 111:1537–1545. [PubMed: 12750403]
5. Alboni P, Gianfranchi L, Brignole M. Treatment of persistent sinus bradycardia with intermittent symptoms: are guidelines clear? Europace. 2009 (doi:10.1093/europace/eup014).
6. Smits JP, Koopmann TT, Wilders R, Veldkamp MW, Opthof T, et al. A mutation in the human cardiac sodium channel (E161K) contributes to sick sinus syndrome, conduction disease and Brugada syndrome in two families. J Mol Cell Cardiol. 2005; 38:969–981. [PubMed: 15910881]
7. Lei M, Huang CL-H, Zhang Y. Genetic Na^+ channelopathies and sinus node dysfunction. Prog Biophys Mol Biol. 2008:171–178. [PubMed: 19027778]
8. Wang DW, Makita N, Kitabatake A, Balser JR, George AL Jr. Enhanced Na^+ Channel Intermediate Inactivation in Brugada Syndrome. Circ Res. 2000; 87:E37–E43. [PubMed: 11029409]
9. Wang DW, Viswanathan PC, Balser JR, George AL Jr, Benson DW. Clinical, genetic, and biophysical characterization of SCN5A mutations associated with atrioventricular conduction block. Circulation. 2002; 105:341–346. [PubMed: 11804990]
10. Abriel H. Roles and regulation of cardiac sodium channel Na_v 1.5: Recent insights from experimental studies. Cardiovasc Res. 2007; 76:381–389. [PubMed: 17727828]
11. Tan BH, Iturralde-Torres P, Medeiros-Domingo A, Nava S, Tester DJ, Valdivia CR, et al. A novel C-terminal truncation SCN5A mutation from a patient with sick sinus syndrome, conduction disorder and ventricular tachycardia. Cardiovasc Res. 2007; 76:409–417. [PubMed: 17897635]
12. Honjo H, Boyett MR, Kodama I, Toyama J. Correlation between electrical activity and the size of rabbit sino-atrial node cells. J Physiol. 1996; 496:795–808. [PubMed: 8930845]
13. Irisawa H, Brown HF, Giles W. Cardiac pacemaking in the sinoatrial node. Physiol Rev. 1993; 73:197–227. [PubMed: 8380502]
14. Lei M, Zhang H, Grace AA, Huang CL. SCN5A and sinoatrial node pacemaker function. Cardiovasc Res. 2007; 74:356–365. [PubMed: 17368591]
15. Zhang H, Holden AV, Kodama I, Honjo H, Lei M, Varghese T, et al. Mathematical models of action potentials in the periphery and center of the rabbit sinoatrial node. Am J Physiol Heart Circ Physiol. 2000; 279:397–421.
16. Zhang H, Holden AV, Noble D, Boyett MR. Analysis of the chronotropic effect of acetylcholine on sinoatrial node cells. J Cardiovasc Electrophysiol. 2002; 13:465–474. [PubMed: 12030529]
17. Zhang H, Zhao Y, Lei M, Dobrzynski H, Liu JH, Holden AV, et al. Computational evaluation of the roles of Na^+ current, i_{Na}, and cell death in cardiac pacemaking and driving. Am J Physiol Heart Circ Physiol. 2007; 292:H165–H174. [PubMed: 16877551]
18. Aslanidi OV, Boyett MR, Dobrzynski H, Li J, Zhang H. Mechanisms of transition from normal to reentrant electrical activity in a model of rabbit atrial tissue: interaction of tissue heterogeneity and anisotropy. Biophys J. 2009; 96:798–817. [PubMed: 19186122]
19. Dobrzynski H, Li J, Tellez J, Greener ID, Nikolski VP, Wright SE, et al. Computer three-dimensional reconstruction of the sinoatrial node. Circulation. 2005; 111:846–854. [PubMed: 15699261]
20. Bleeker WK, Mackaay AJ, Masson-Pevet M, Bouman LN, Becker AE. Functional and morphological organization of the rabbit sinus node. Circ Res. 1980; 46:11–22. [PubMed: 7349910]
21. Alings AM, Bouman LN. Electrophysiology of the ageing rabbit and cat sinoatrial node - a comparative study. Eur Heart J. 1993; 14:1278–1288. [PubMed: 8223742]
22. Lei M, Jones SA, Liu J, Lancaster MK, Fung SS-M, Dobrzynski H, Camelliti P, Maier SKG, Noble D, Boyett MR. Requirement of neuronal- and cardiac-type sodium channels for murine sinoatrial node pacemaking. J Physiol (Lond.). 2004; 559:835–848. [PubMed: 15254155]

23. Protas L, Oren RV, Clancy CE, Robinson RB. Age-dependent changes in Na^+ current magnitude and TTX-sensitivity in the canine sinoatrial node. J Mol Cell Cardiol. 2010; 48:172–80. [PubMed: 19665465]
24. Lyashkov AE, Vinogradova TM, Zahanich I, Li Y, Younes A, Nuss HB, Spurgeon HA, Maltsev VA, Lakatta EG. Cholinergic receptor signaling modulates spontaneous firing of sinoatrial nodal cells via integrated effects on PKA-dependent Ca^{2+} cycling and I_{KACh}. Am J Physiol. 2009; 297:H949–H959.
25. Shaw RM, Rudy Y. Ionic mechanisms of propagation in cardiac tissue: roles of the sodium and L-type calcium currents during reduced excitability and decreased gap junction coupling. Circ Res. 1997; 81:727–741. [PubMed: 9351447]
26. Tateyama M, Liu H, Yang A-S, Cormier JW, Kass RS. Structural effects of an LQT-3 mutation on heart Na^+ channel. Biophys J. 2004; 86:1843–1851. [PubMed: 14990510]
27. Mantegazza M, Yu FH, Catterall WA, Scheuer T. Gating role of the C-terminal domain in inactivation of brain and cardiac sodium channels. PNAS. 2001; 98:15348–15353. [PubMed: 11742069]
28. Boyett MR, Holden AV, Kodama I, Suzuki R, Zhang H. Atrial modulation of sinoatrial pacemaker rate. Chaos Soliton Fract. 1995; 5:425–438.
29. Han X, Kobzik L, Severson D, Shimoni Y. Characteristics of nitric oxide-mediated cholinergic modulation of calcium current in rabbit sinoatrial node. J Physiol. 1998; 509:741–754. [PubMed: 9596796]
30. Petit-Jacques J, Bois P, Bescond J, Lenfant J. Mechanism of muscarinic control of the high-threshold calcium current in rabbit sino-atrial node myocytes. Pflugers Arch. 1993; 423:21–27. [PubMed: 8387668]
31. Kurata Y, Matsuda H, Hisatome I, Shibamoto T. Regional difference in dynamical property of sinoatrial node pacemaking: role of Na^+ channel current. Biophys J. 2008; 95:951–77. [PubMed: 18390617]

Europe PMC Funders Author Manuscripts

Europe PMC Funders Author Manuscripts

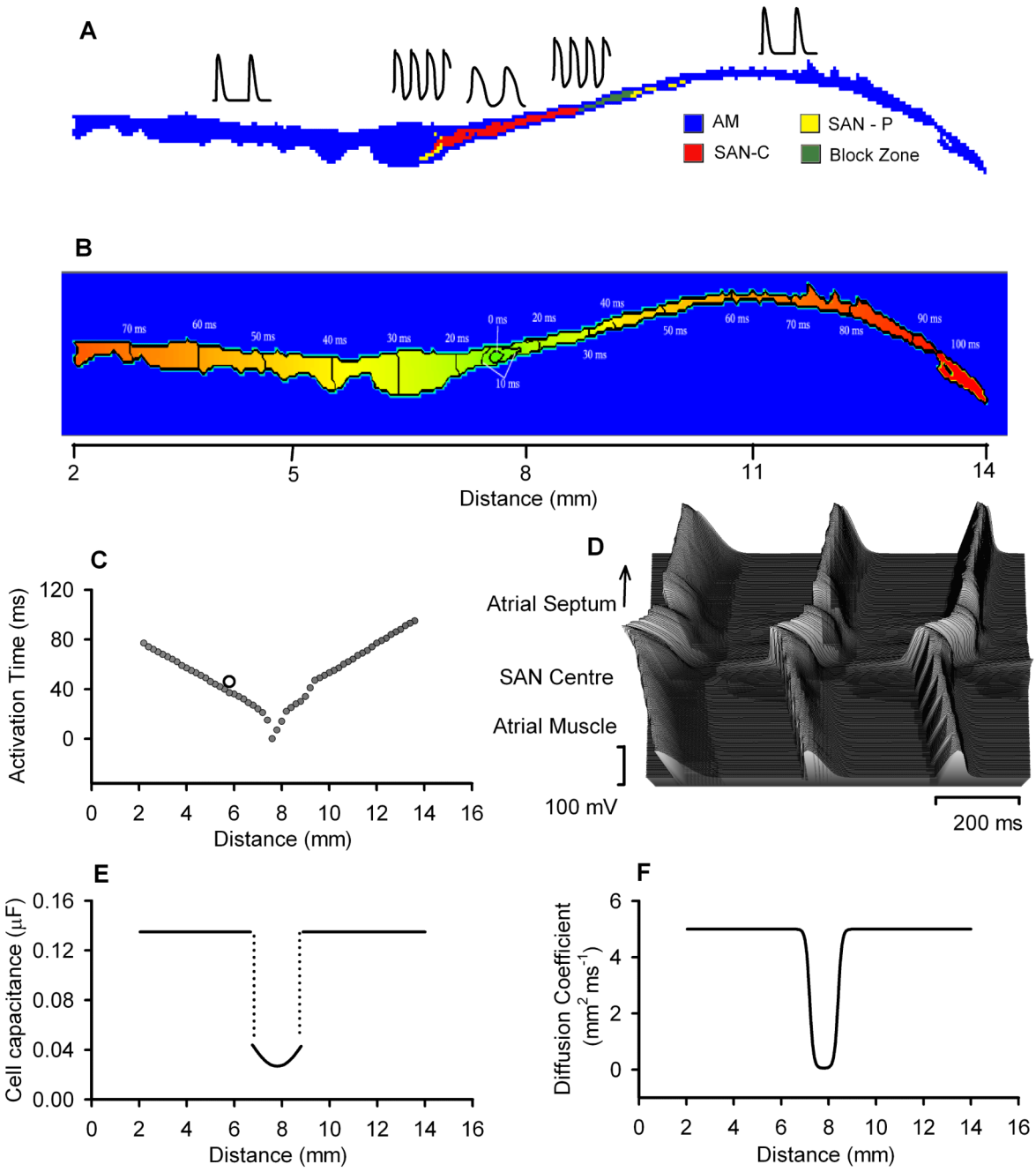

Figure 1.

Model of the rabbit SAN and surrounding atrial tissue. A: colour-coded distribution of cell types throughout the 2D tissue slice. Insets show respective single cell APs. B: spatial distribution of the activation time during normal AP conduction through the 2D slice (rainbow palette). Lines are isochrones and numbers are activation time in ms. C: activation time profile through the middle of the 2D slice; an open circle shows respective experimental data.[21] D: AP profiles during conduction through the slice. E: gradient in cell capacitance along the slice. F: gradient in the diffusion coefficient along the slice.

Europe PMC Funders Author Manuscripts

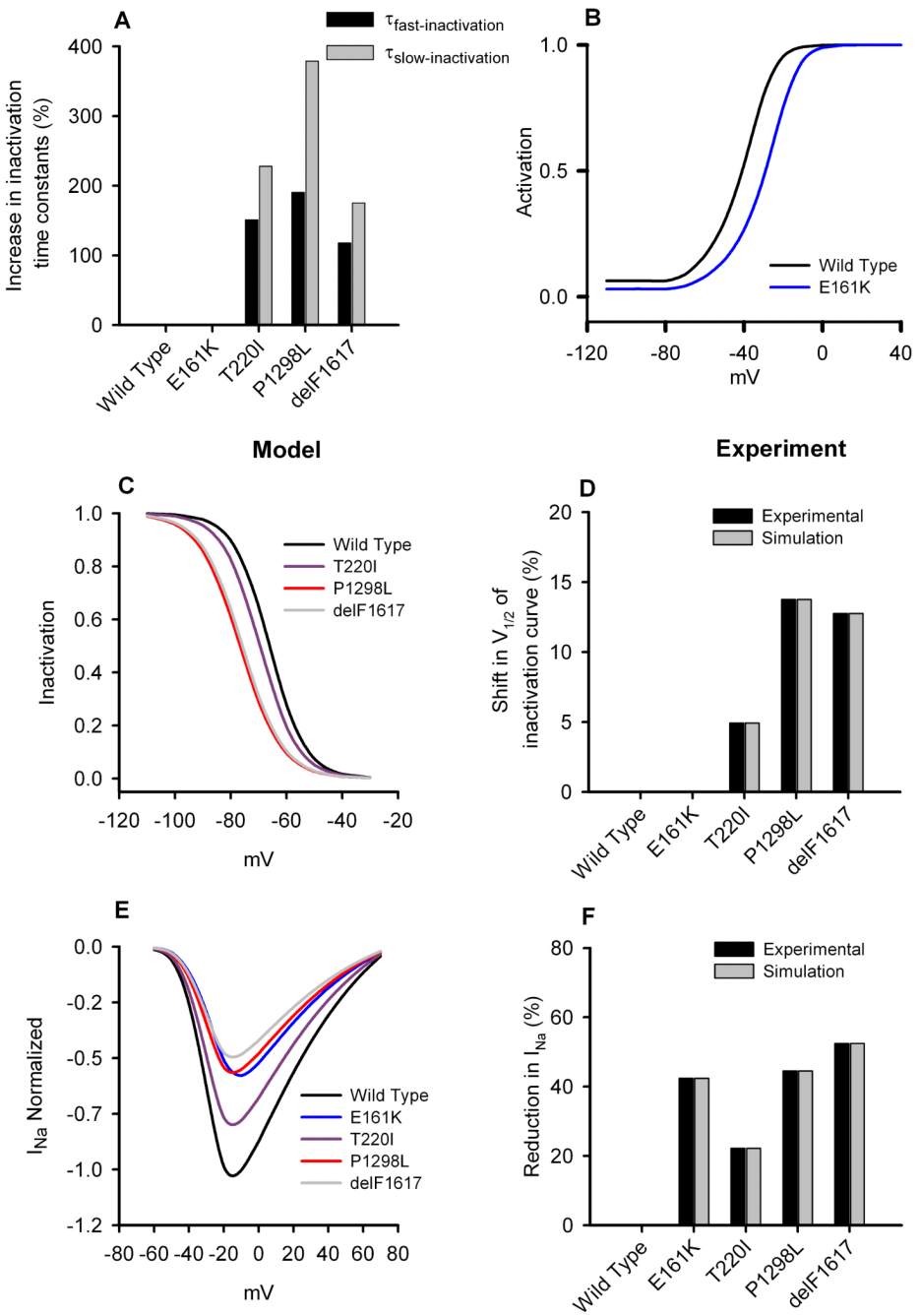

Figure 2.

Effects of the SCN5A mutations on Na^+ current in SAN cells. A: percentage increase of the fast and slow Na^+ channel inactivation time constants from the WT channel to T220I, P1298L, delF1617 and E161K mutant channels. B: simulated steady-state activation curve for Na^+ channel. C: simulated steady-state inactivation curves for Na^+ channel. D: relative (to the WT channel) shift of the steady-state inactivation curve from experimental data. E: normalised simulated Na^+ channel current density. E: percentage reduction in Na^+ current density from the WT channel. For mutation parameter values see Online Table I.

Europe PMC Funders Author Manuscripts

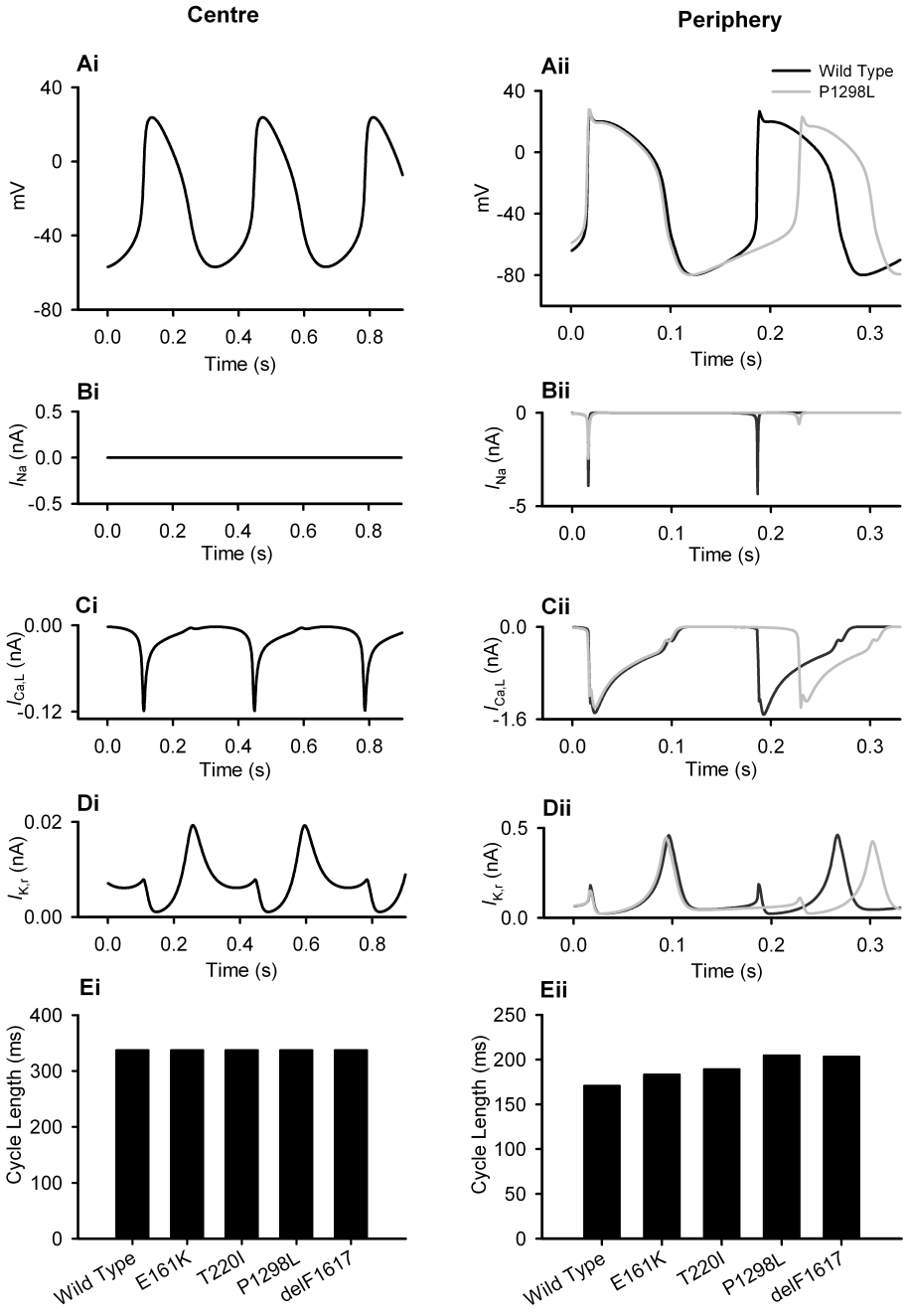

Figure 3.

Effects of the SCN5A mutations on the SAN pacemaking rate. Simulated voltage and current recordings from central (i) and peripheral (ii) SAN cells. Effects of the mutation on APs (A), I_{Na} (B), $I_{Ca,L}$ (C), $I_{K,r}$ (D) and PCL (E) shown.

Europe PMC Funders Author Manuscripts

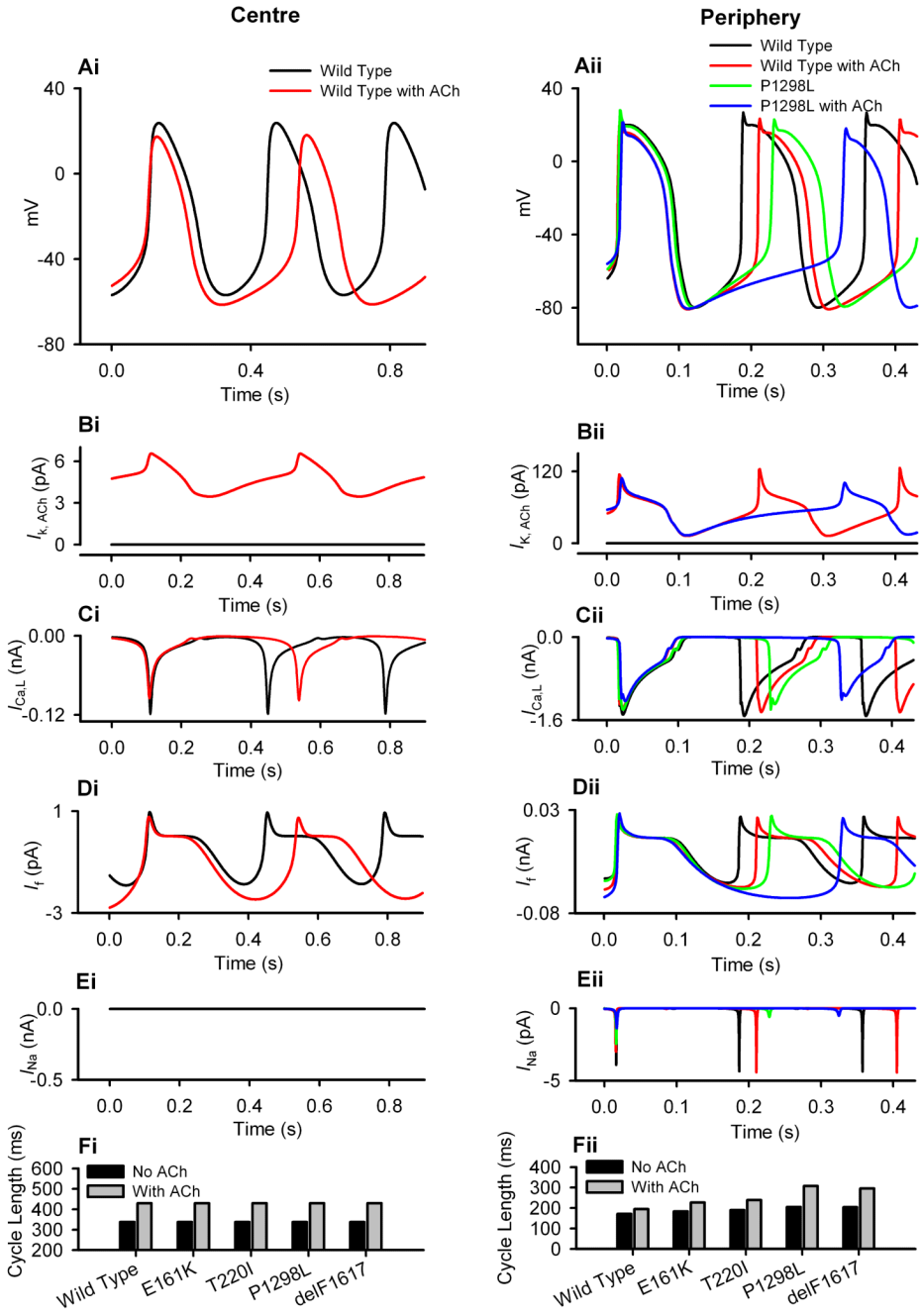

Figure 4.

Effects of ACh on the SAN pacemaking rate. Simulated voltage and current recordings from central (i) and peripheral (ii) SAN cells. Effects of the SCN5A mutations and [ACh] = 1.5 $\times 10^{-8}$ mol/L on APs (A), $I_{K,ACh}$ (B), $I_{Ca,L}$ (C), I_f (D), I_{Na} (E) and PCL (F) shown.

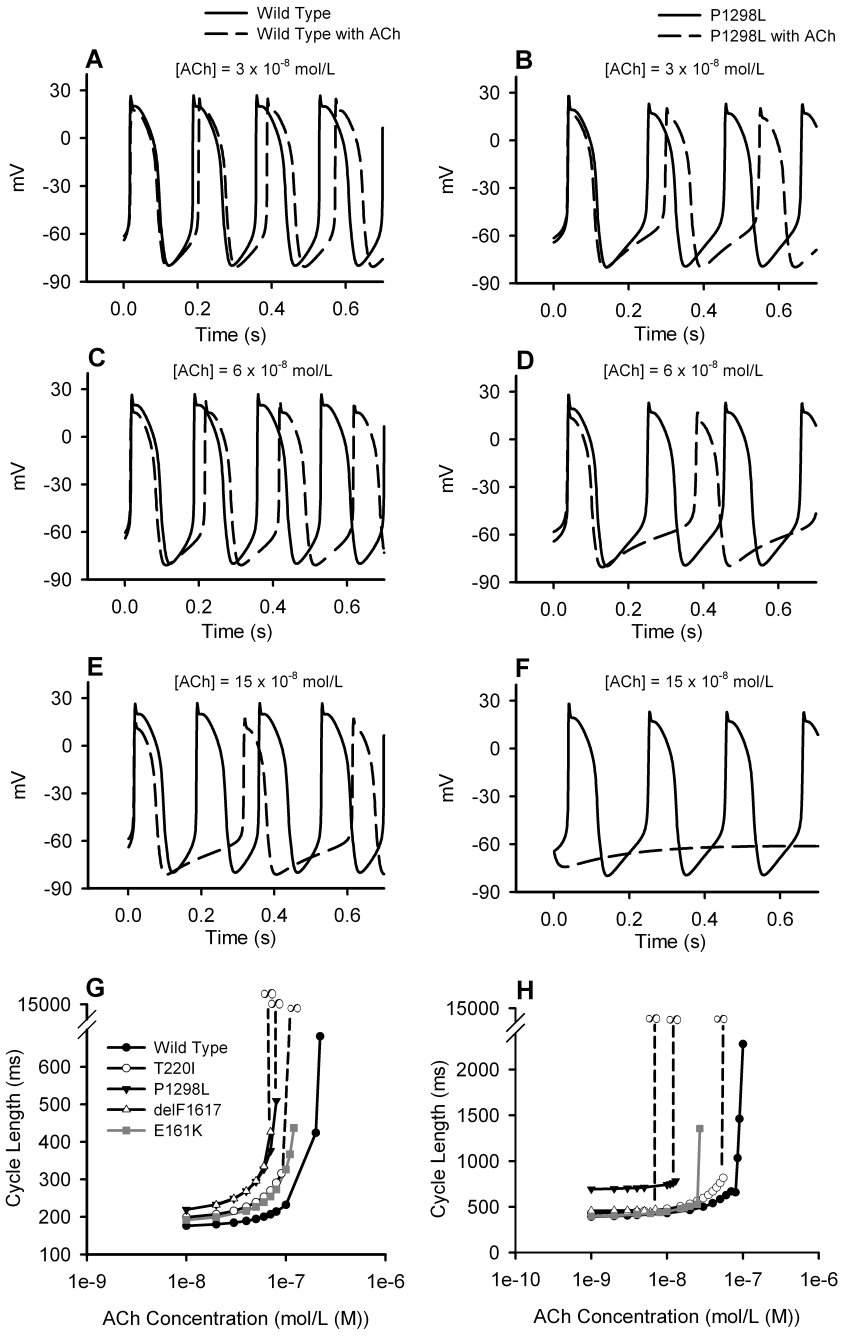

Figure 5.

Effects of ACh and the SCN5A mutations on the SAN pacemaking rate. A-F: effects of varying ACh concentrations on AP generation in SAN cells with the WT (left) and mutant (right) channels. G: dependence of PCL on ACh concentration in single cell simulations. H: dependence of PCL on ACh concentration in 2D simulations.

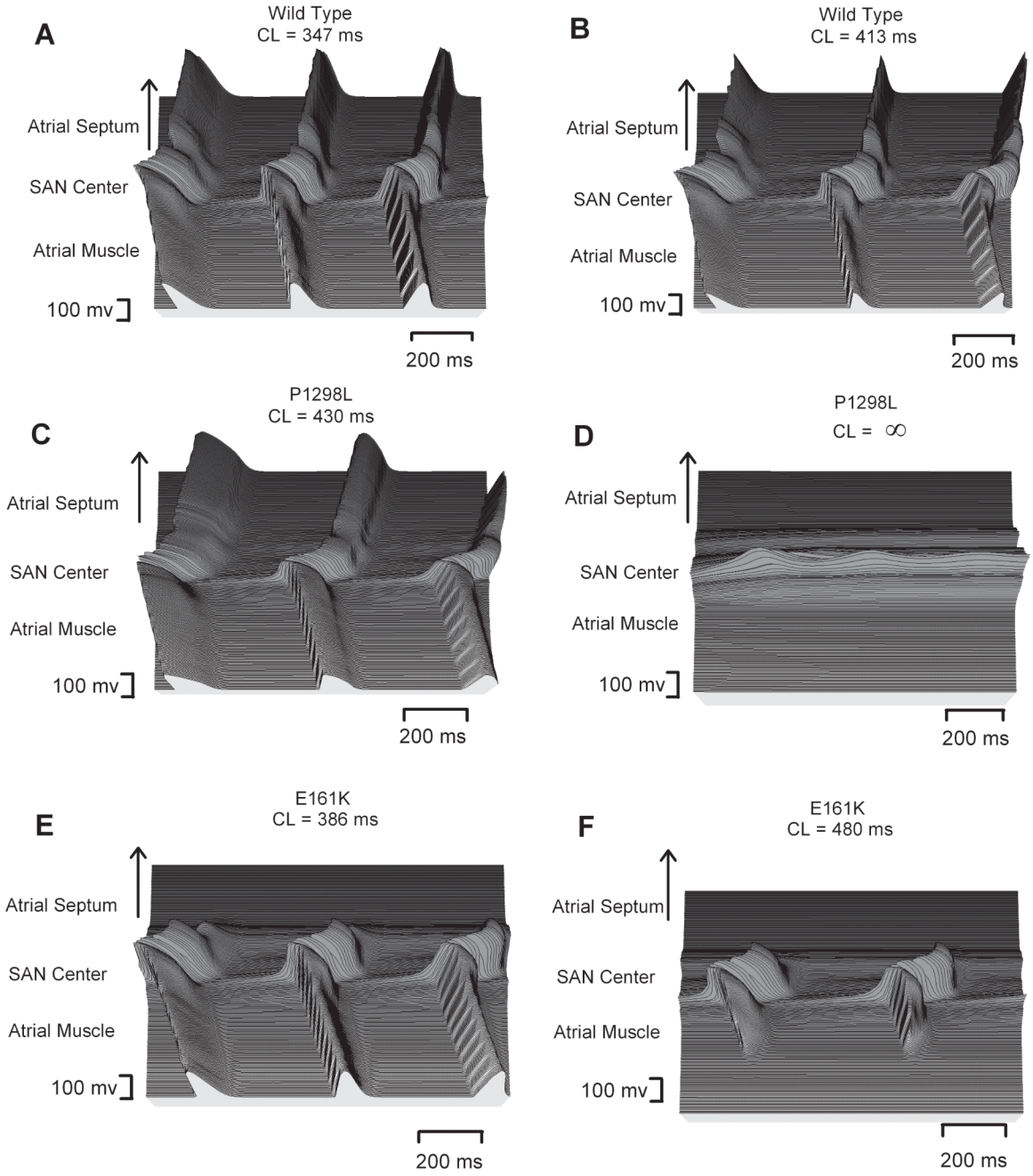

Figure 6.

Effects of ACh and the SCN5A mutations on AP conduction. AP profiles in the 2D tissue with [ACh] = 0 (left) and [ACh] = 1.5×10^{-8} mol/L (right) are shown. A, B: tissue with the WT channel. C, D: tissue with the P1298L mutant channel. E, F: tissue with the E161K mutant channel.

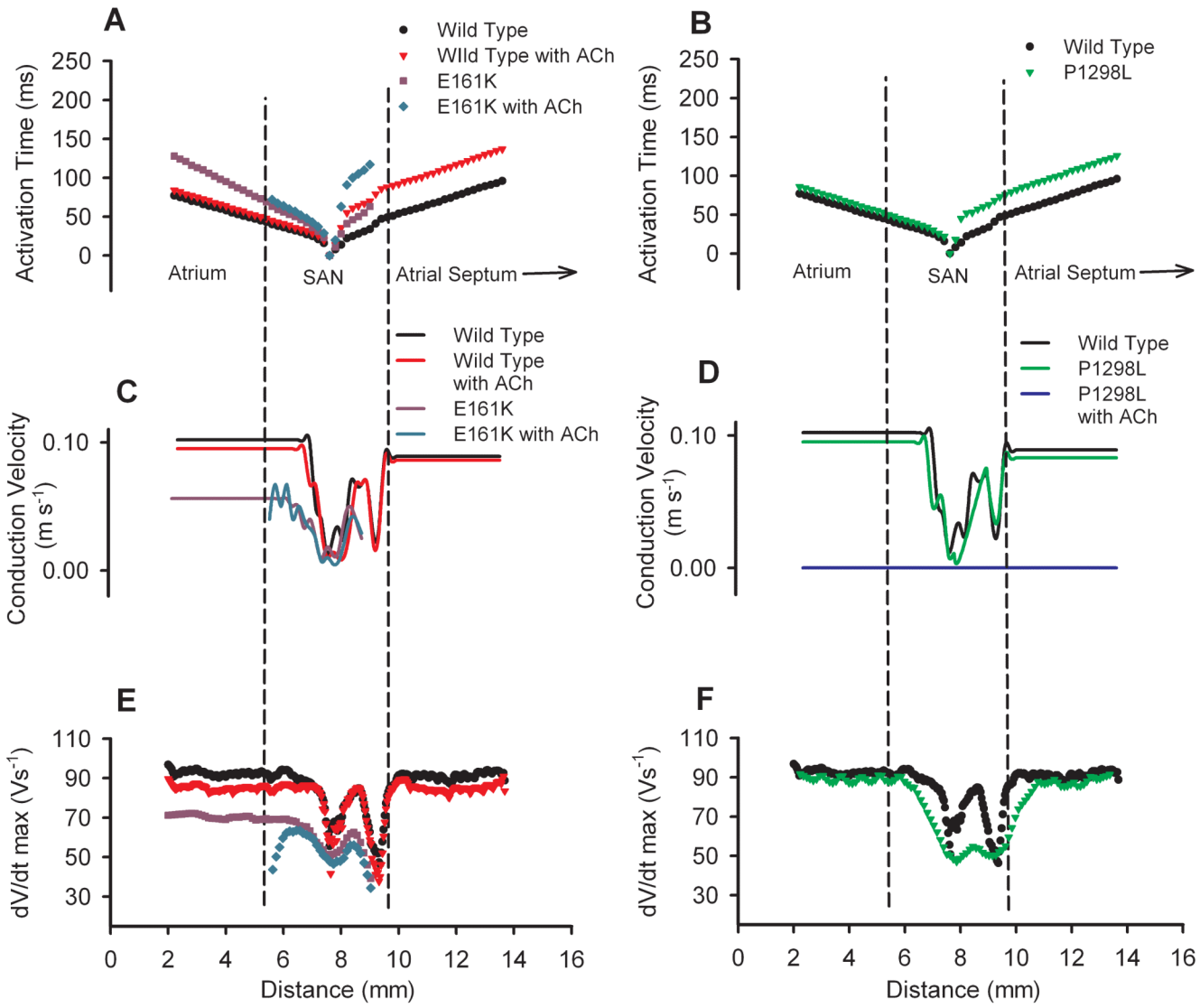

Figure 7.

Effects of ACh and the SCN5A mutations on AP conduction parameters: activation times with the E161K mutation and ACh (A) and the P1298L mutation (B) as compared to the WT channel; conduction velocities with the E161K mutation and ACh (C) and the P1298L mutation (D) as compared to the WT channel; dV/dt_{max} with the E161K mutation and ACh (E) and the P1298L mutation (F) as compared to the WT channel. [ACh] = 1.5×10^{-8} mol/L.

Europe PMC Funders Author Manuscripts

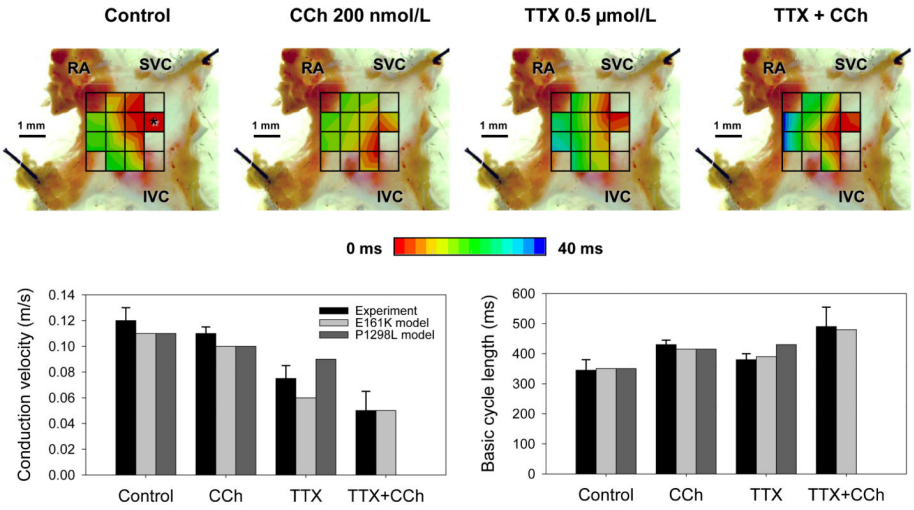

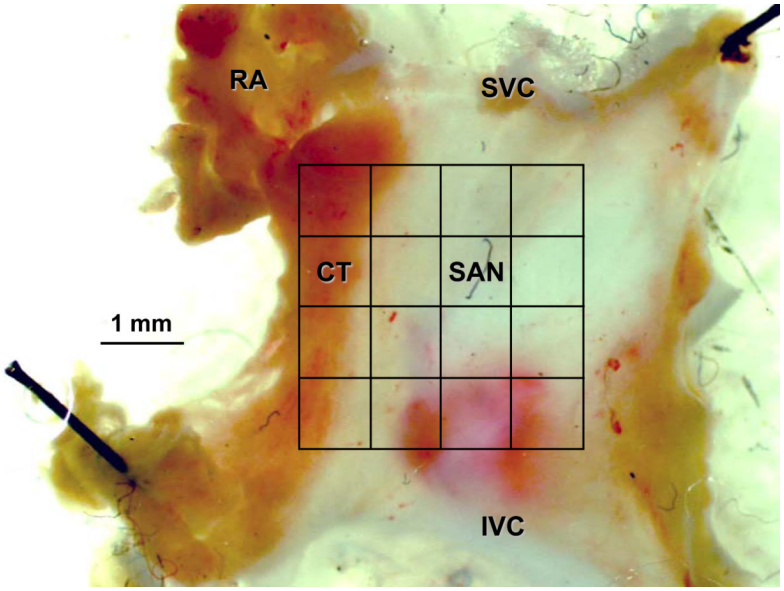

Europe PMC Funders Author Manuscripts

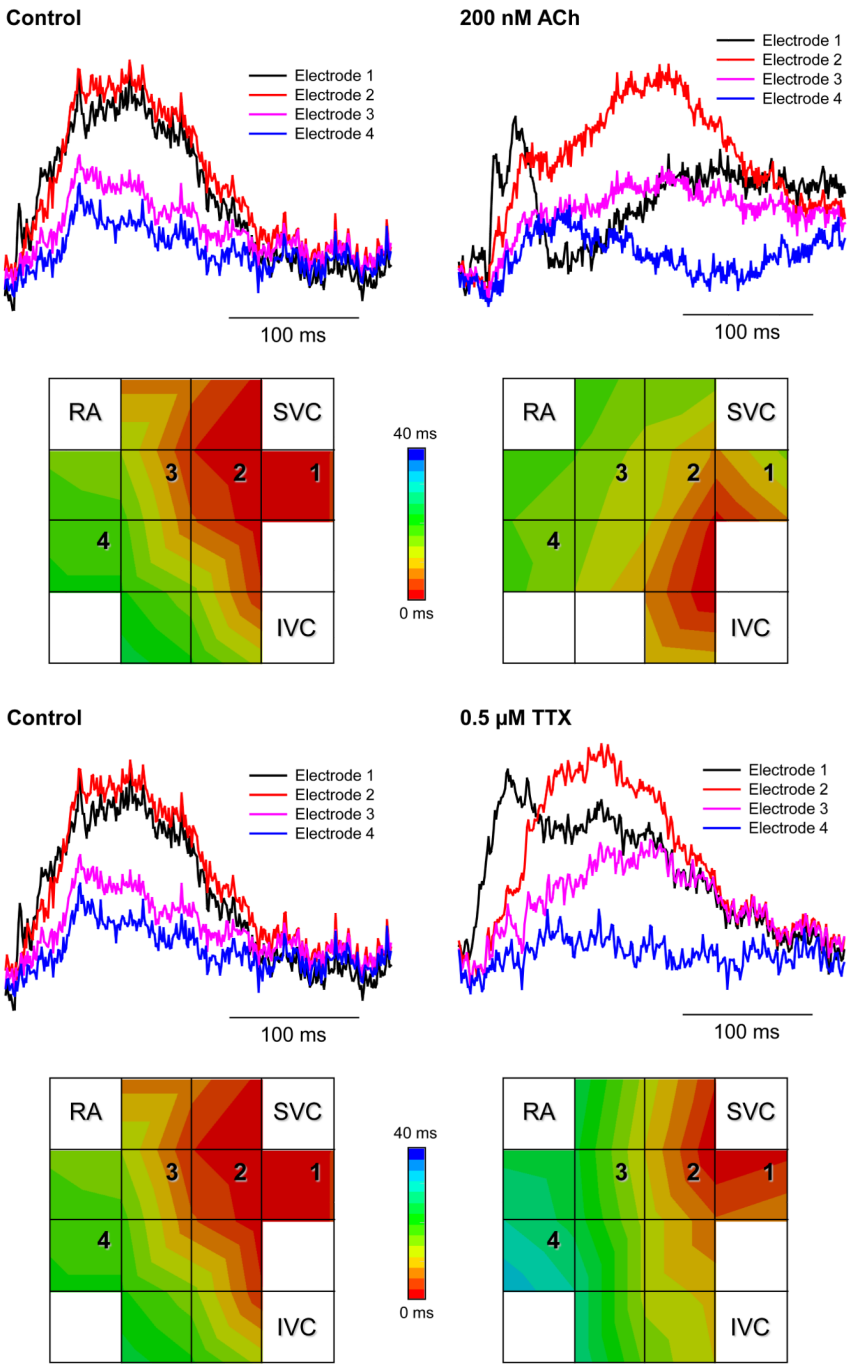

Europe PMC Funders Author Manuscripts

Europe PMC Funders Author Manuscripts

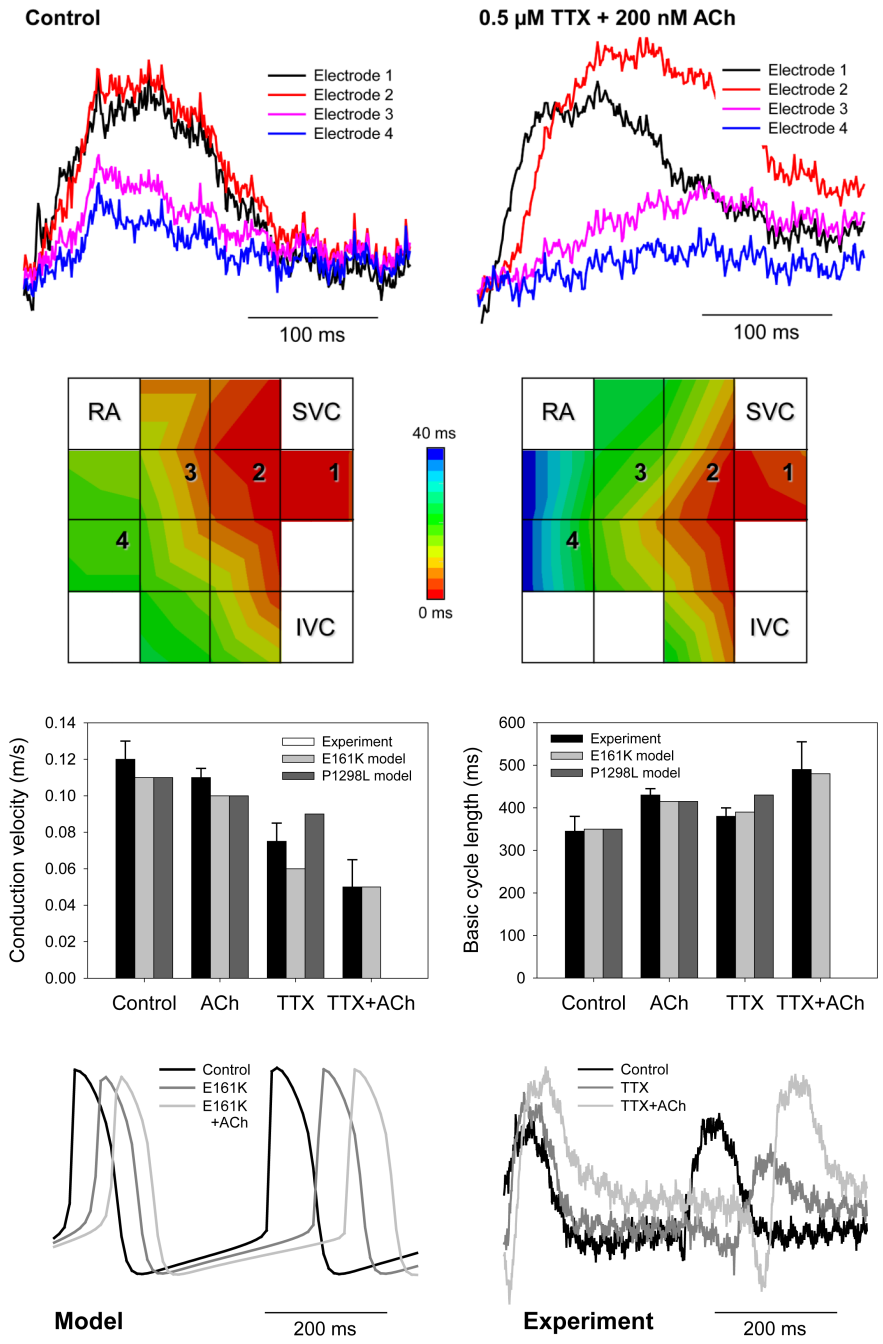

Figure 8.

Experimental validation of the SAN-atrium tissue model. Isolated SAN-atrium tissue with superimposed activation maps (top) show increase of the conduction time from the SAN into the RA due to effects of TTX, CCh and their combination (see panel labels). AP conduction velocities and PCLs under all conditions considered match the respective values simulated with the 2D tissue model (bottom). SVC – superior vena cava, IVC – inferior vena cava. The SAN leading pacemaker cite in control is shown with an asterisk.